Northumbria Research Link

Northumbria
University
NEWCASTLE

Determination of Stray Inductance of Low Inductive Laminated Planar Multi-Port Busbars using Vector Synthesis Method

Binxian Lu, *Member, IEEE*, Volker Pickert. *Member, IEEE*, Junzhu Hu, Haimeng Wu *Member, IEEE, R. T. Naayagi, senior Member, IEEE,* Wei Kang, Sizhuo Liao

***Abstract*— Laminated busbars connect capacitors with switching power modules and they are designed to have low stray inductance to minimize electromagnetic interference. Attempts to accurately measure the stray inductance of these busbars have not been successful. The challenge lies with the capacitors as each of them excite the busbar producing their individual stray inductances. These individual stray inductances cannot be arithmetically averaged to establish the total stray inductance that applies when all the capacitors excite the busbar at the same time. It is also not possible to measure the stray inductance by simultaneous excitation of each capacitor port using impedance analyzers. This paper presents a solution to the above dilemma. A vector synthesis method is proposed whereby the individual stray inductance from each capacitor port is measured using an impedance analyzer. Each stray inductance is then mapped into an *x-y-z* frame with a distinct direction. This mapping exercise allows the data to be vectored. The total stray inductance is then the sum of all the vectors. The effectiveness of the proposed method is demonstrated on a busbar designed for H-bridge inverters by comparing the simulation and practical results. The absolute error of the total stray inductance between the simulation and the proposed method is 0.48nH. The proposed method improves the accuracy by 14.9% compared to the conventional technique in measuring stray inductances.**

***Index Terms*— planar busbar, stray inductance, measurement, impedance analyzer, vector synthesis method, H-bridge inverter**

I. INTRODUCTION

Voltage source inverters such as the H-bridge inverter are commonly used in electric drives applications [1-3]. An H-bridge inverter requires the input dc-link capacitance to stabilize the input voltage.

Manuscript received April 26, 2018; revised October 6, 2018 and December 20, 2018; accepted January 27, 2019.

Binxian Lu and Sizhuo Liao are with the School of Electrical and Electronic Engineering, North China Electric Power University, Beijing, China

V. Pickert and H. Wu are with the School of Engineering, Newcastle University, Newcastle upon Tyne, United Kingdom. R. T. Naayagi is with Newcastle University in Singapore (NUiS), Singapore. (Corresponding author: Haimeng Wu and Binxian Lu, phone: +44 (0) 1912087588, emails: haimeng.wu@ncl.ac.uk, lbx@ncepu.edu.cn).

Junzhu Hu is with State Grid Beijing Changping Electric Power Supply Company, Beijing, China and Wei Kang is with Global Energy Interconnection Research Institute, Beijing, China

In practical applications, several capacitors are connected in parallel in order to achieve the required capacitance and to reduce the current stress for each capacitor [4]. All of the dc-link capacitors are connected to the busbar which connects them with the power switching modules and the voltage sensor measuring the dc-link voltage.

The preferred busbar type for H-bridge inverters is the laminated planar busbar. Laminated planar busbars are made in a sandwich arrangement where an insulating material (commonly epoxy glass or Mylar) is sandwiched between two metal plates (commonly copper or aluminum). One metal plate is positively charged and the other is negatively charged. The gap between the plates is determined by the thickness of the insulator and it varies between 0.2 mm and 6 mm depending on the maximum applied voltage level across the busbar [5]. This arrangement of thin parallel metal plates laminated with a thin dielectric enables to minimize the effect of stray inductance [6]. It is well known that stray inductances greatly influence the operation of H-bridge inverters. For example, during switching transients, stray inductances are responsible for increasing the switching losses [7], producing electromagnetic interference [8], and during turn-off, the stray inductances cause voltage stress across the power switching devices [9]. Consequently, in order to ensure a good switching performance, it is essential to design a laminated planar busbar with low stray inductance [10-12].

To demonstrate a good busbar design the stray inductance must be validated by experiment. Two measurement methods can be applied: indirect and direct. The indirect method measures the voltage overshoot ΔV and the current change $\mathrm{d}i/\mathrm{d}t$ to calculate the stray inductance value of the current commutation loop [13]. This practical approach requires that the busbar is physically connected with the charged capacitors and the power switching module that is turned on and turned off. Tests can be conducted in the fully assembled inverter or more commonly in a double pulse tester [14]. Reference [11] suggested an improvement to the double pulse test by adding a resonant capacitor to measure the stray inductance. However, methods, where the busbar is energized and physically connected with the dc-link capacitors, result in the measurement of the stray inductance of the whole loop. Thus, the individual stray inductance of the busbar cannot be filtered away from the stray inductance of the capacitors and the power device. To overcome this [15] suggested calculating the parasitic inductance of a busbar by injecting current into the

busbar which is physically connected to the circuit. The voltage is then measured across the DC link busbar allowing the calculation of the stray inductance. This technique, however, requires additional circuitry and the high frequency contents of the injected current can also flow through the capacitors and the anti-parallel connected diodes within the power switching modules thus measuring their inductances too. Reference [16] systematically studied the stray inductance of laminated busbars both analytically and by experiment. The authors presented a resonance measurement method for measuring the low stray inductance. Step-by-step measurements along the busbar are required resulting in a cumbersome measurement procedure. Based on the studies reported thus far, all the indirect measurement methods lag in terms of the accuracy and are time-consuming. Therefore, the indirect method is not preferable for measuring the stray inductances of busbars.

The direct measurement method is a good alternative and requires special equipment. Three equipment types can be used: LCR meter [17], impedance analyzer [6] and network analyzer [18]. Using any of these equipment does not require the connection of charged capacitors to the busbars or the connection to power switching modules. Only the busbar is connected to the equipment. Fundamentally an LCR meter and an impedance analyzer are similar as both measure the impedance of a busbar. This is achieved by measuring the voltage-to-current ratio which is phase-sensitive [19] and this ratio represents the fundamental impedance value of the busbar. From this value, the stray inductance of the busbar can be calculated. An LCR meter conducts the impedance measurement at one frequency only, whereas an impedance analyzer offers the capability to sweep the frequency thus an impedance spectrum can be displayed providing information on how the stray inductance varies over a frequency range. A network analyzer injects an incident signal into the busbar and captures the reflected signal. From both these signals, the reflected coefficient is calculated and this coefficient is processed to determine the frequency response of the busbar impedance.

In order to measure the stray inductance, the measurement equipment is connected to the busbar port that connects to the dc-link capacitor and an excitation signal is injected at the point where the dc-link capacitor is connected to. This approach, however, is known for errors which have been reported in the literature [20]. The error is caused as the equipment can only be connected to one port that connects to the dc-link capacitor. Busbars that connect several capacitors have several ports and the question is which port to choose from to determine the stray inductance.

Although it is possible to measure the stray inductances individually at each port that a capacitor is connected to, the individual stray inductances cannot be arithmetically added to represent the total stray inductance of the busbar [21]. Also, practically, it is not possible to operate several of the same equipment types in parallel (for each dc-link capacitor port one analyzer) to measure the total stray inductance as each equipment would interfere with each other. Therefore, the common approach is to assume that all capacitors are connected in the geometrical center of the busbar. The port that is closest to the center is used for measurement. The stray inductance of this measurement represents the stray inductance of the busbar. Clearly, this value is not a true representation as excitation takes place at each port that a capacitor is connected to. Of the three equipment discussed for the stray inductance measurement, the impedance analyzer is preferable as it is low cost compared to the network analyzer [22] and is easier to use than an LCR meter for performing frequency sweep.

This paper addresses a practical challenge of measuring the stray inductance of a laminated planar busbar. The proposed method is based on data mapping and vector synthesis theory. The stray inductance of each capacitor port is measured individually and then an analytical method has been developed to calculate the total stray inductance order from the measured data. This study is conducted on a low stray inductance laminated planar busbar which is designed for a single-phase voltage source H-bridge inverter. The comparison of the analytical results and Finite Element Method (FEM) simulation are given in detail and the experimental validation is also provided.

The paper is structured as follows. Section 2 describes the design of a low stray inductance laminated planar busbar and gives the FEM results and the values of stray inductances. Section 3 introduces the analytical method to calculate the total stray inductance and compares the calculated total stray inductance with the FEM results. Section 4 describes the experimental setup and test results followed by Section 5 which discusses the analytical results and compares them with the FEM simulations and experimental results. Finally, the conclusions are drawn in Section 6.

II. Design of a Low Inductance Busbar and FEM Simulation Results

A. Description of a low inductive laminated planar busbar

For the measurement of stray inductance, two commercial low inductance laminated planar busbars are used which are labeled as busbar A and busbar B and their geometries are shown in Fig. 1(a) and Fig. 1(b), respectively. The busbar A has 20 ports and the corresponding port numbers are indicated in Fig 1(a). The busbar B has 25 ports and the corresponding port numbers are indicated in Fig 1(b). These two busbars are designed with the rated power of 1100V/150A and 1100V/270A, respectively, which can be used for power conversion of DC to AC, powering an inductive load. The busbars play a role as a connection of capacitors and power switches modules with a structure of two conductive copper layers and several insulated polyimide layers as shown in Fig.1 (c). The schematic of the power circuit is shown in Fig. 1 (d). The anode and the cathode of capacitors are connected with the positive and negative plates of the busbars in Fig. 1(a) or Fig. 1(b), respectively. For busbar A, Port 17 forms the first leg of the H-bridge inverter in the modular multilevel converter (MMC) and connects to a power switching module

that contains two IGBT power switches with antiparallel diodes connected in a half bridge (S_1 and S_3). Port 19 connects the second leg of the H-bridge converter (S_2 and S_4). They have been shown in the right part of Fig. 1(d). For analysis, Port 19 is defined as the reference point and therefore all the described stray inductances in this paper refer to Port 19. This implies Port 19 must be short-circuited. The short circuit link should be designed to provide good electrical contact but also should have low stray inductance. A piece of copper with a width of 7mm, a thickness of 1mm and length of 22mm has been added and these values have been used for practical measurement and simulation. Port 16 and Port 18 form connections to the high frequency filter capacitors C_{o1} and C_{o2}. Fig 1(a) shows that Ports 16 and 17 and Ports 18 and 19 are 180 mm apart and each of the ports is 120mm away from the edge of the plates. Port 20 is used to measure the DC voltage. Note that this port is bent upwards to avoid electromagnetic interference from the busbar. Although bending adds a stray inductance with regard to Port 20, measurement of the dc-link is an average voltage and so the impact on the additional stray inductance can be ignored. In Fig 1(a) the upper plate is defined as positive and the lower plate is defined as negative. The plates are made of copper. The width of each plate is 420mm, the length is 265mm, the thickness is 2mm, and the spacing between the positive and negative plates is p=0.5 mm. Fig. 1 (b) shows that the busbar has two insulating layers each with a thickness of 0.25 mm between the positive and the negative plates. In addition, an insulation layer is placed on top of the positive rail and the bottom of the negative rail to avoid breakdown at the edge of plates. The insulation material used is polyimide and its relative permittivity is 4. Hot-pressing [23] was used to build the planar busbar.

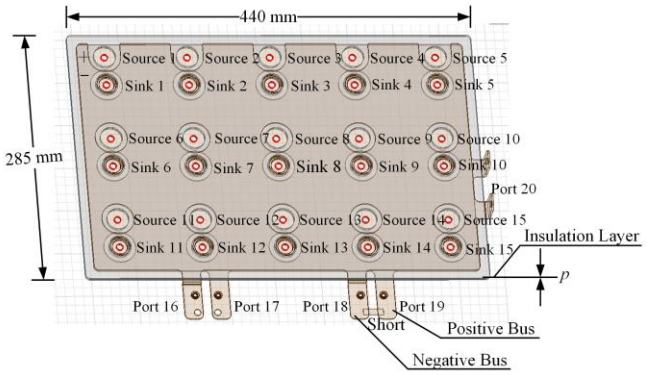

(a)

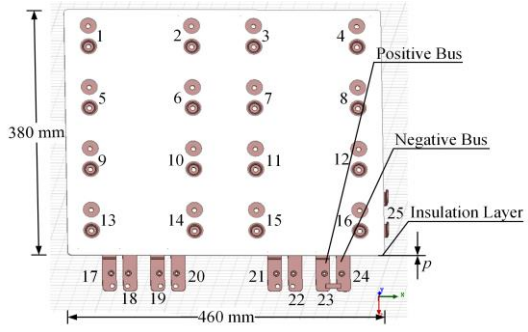

(b)

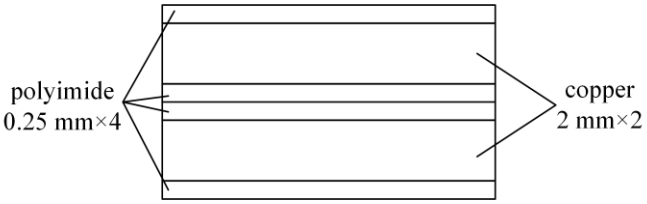

(c)

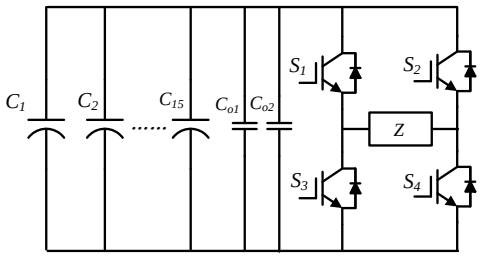

(d)

Fig. 1 (a) A Low inductance laminated planar busbar A with 20 ports (1100V/150A). (b) A Low inductance laminated planar busbar B with 25 ports (1100V/270A). (c) A Cross-sectional view of the busbar model. (d) Diagram of single phase H-bridge inverter

B. MOM Simulation

The busbar is shown in Fig. 1(a) has been incorporated and simulated in ANSYS Q3D Extractor™ to calculate the stray inductances. ANSYS Q3D Extractor™ performs 3-D quasi-static electromagnetic field simulations. It is possible to excite just one of the fifteen ports (Port 1 to Port 15) that connect to the dc-link capacitors C_1 to C_{15} respectively to establish the stray inductance individually or all the ports (Port 1 to Port 15) may be excited at the same time to generate the total stray inductance of the busbar.

ANSYS Q3D Extractor™ provides electromagnetic field simulation tools which employ Moment of Method (MOM) to solve Maxwell's integral field equations. The total grid number of 153,595 was applied for each port (Port 1 to Port 15) for calculation of the stray inductance. The grid was applied across the two copper planes (top, bottom). The computation time for each port took approximately 25 minutes until the full convergence was achieved. The computer used was an Intel i7 core with RAM memory of 32GB (i7-3920XM CPU 3.1GHz). Each port was excited with a small amplitude AC signal of 841kHz. This frequency corresponds to a 1.2 μs device turn-off time chosen as for this research.

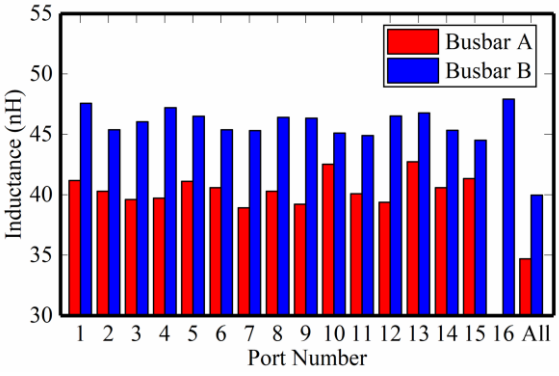

Fig.2 Simulated inductances in ANSYS Q3D ExtractorTM at different ports for busbar A and busbar B（unit: nH）

Fig.2 shows the results for each stray inductance at different ports for busbar A and busbar B. All stray inductances are only several tens of nH confirming that this design is of low inductance. The lowest stray inductance is measured from Port 7 (38.911nH) and the highest value is measured from Port 13 (42.741nH) for busbar A. The maximum difference between the simulated stray inductances is therefore 3.83nH. The lowest stray inductance is measured from Port 15 (44.5211nH) and the highest value is measured from Port 16 (47.928nH) for busbar B. And the maximum difference between the simulated stray inductances is therefore 3.407nH. Fig.2 also shows the result of the total stray inductance resulting from the simulation when all the ports are excited simultaneously. The value is 34.699nH and 39.957nH respectively for busbar A and busbar B which are much lower compared to any of the individual measured stray inductances. This result supports the statement that the total stray inductance cannot be arithmetically averaged across all individual stray inductances.

Fig.2 shows that depending on where the impedance analyzer is connected, the inductance value would differ and the same was observed during experimentation.

III. Analytical Calculation of the Total Stray Inductance

A. Analytical calculation of the total stray inductance

In this paper, we study the inductance measurement and synthesis methods mainly based on busbar A. ANSYS Q3D Extractor™ calculated a total stray inductance of 34.699nH. This value is based on the fact that all the 15 ports were excited at the same time. Practically, exciting and measuring 15 ports with 15 impedance analyzers is infeasible. Therefore, a method is proposed that analytically calculates the total stray inductance based on the individual measurements at each port using vector synthesis method. To apply this method, each connection between any of the Ports 1 to 15 and Port 19 is approximately represented as a parallel flat conductor as shown in Fig. 3

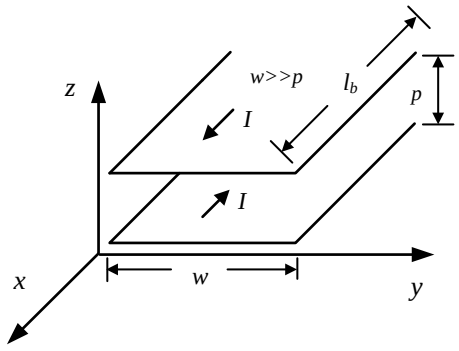

Fig. 3 Parallel flat conductor

In Fig. 3, the width w and length l_b of the plates is much larger than the spacing between the two plates, p, and assume current density on surface of plate is uniform, thus end effect and fringing effect of magnetic field are neglected, and the magnetic field H has only a y-orientation, H_y, and the current I can be expressed as,

$$I = \int_0^w H_y dy = H_y w \tag{1}$$

The magnetic flux ϕ is:

$$\phi = \int_0^p \int_0^{l_b} \frac{\mu I}{w} dz dx = \frac{\mu I}{w} p l_b = LI \tag{2}$$

Where μ is the permeability. From (2) the inductance L is:

$$L = \frac{\mu p l_b}{w} \tag{3}$$

Equation (3) can be applied to all the ports resulting in 15 individual stray inductances (L_1 to L_{15}). However, these inductances cannot be arithmetically added to calculate the total stray inductance. This is because (3) applies to the reference frame (x-y-z) that describes the alignment between the excited port and Port 19. As the busbar has 15 ports, 15 individual reference frames (x_1-y_1-z_1 to x_{15}-y_{15}-z_{15}) with respect to Port 19 apply. In order to calculate the total stray inductance, each reference frame must be aligned with respect to one master reference frame (x_0-y_0-z_0).

Actually, from the electromagnetic field point of view inductance can be seen as an equivalent parameter.

$$L = \frac{\phi}{i} \tag{4}$$

Where ϕ is magnetic flux. Here, a single turn is considered. This supposition is in agreement with that prescribed in this paper. According to the relationship of the flux linkage with magnetic induction intensity, there is

$$L = \frac{\int \vec{B} \cdot d\vec{s}}{i} \tag{5}$$

Due to the problem of the inductance of busbar being linear, superposition theorem can be used to calculate the total flux linkage by summing flux linkage generated by currents excited by individual ports. So,

$$L = \frac{1}{15i} \sum B_j \Delta s_j cos\theta \tag{6}$$

Here we assume excited currents at individual ports are all equal to i. If let i be unit, inductance is the summation of products of a differential surface with a project of magnetic induction intensity on the normal direction of this differential surface. It is equivalent to a summation of vectors. The total inductance of busbar described above is analogous to this summation procedure. If total current is applied at an equivalent port in Fig. 4(a) it can be divided into 15 currents to every sub-port on the low busbar plates. In Fig. 4(a) one terminal of sub-port is corresponding to one terminal of the current distributor from number 1 to 15. All the other terminals at individual ports are joined together and connected with a return output terminal of the current distributor, terminal 16. Therefore, there are 16 terminals at the output of the distributor. From electromagnetic respect, the total inductance can be obtained in three steps. The total magnetic induction intensity is first resolved through vector summation of magnetic induction intensity generated by every sub-port

current. Then the total magnetic flux can be calculated by surface integral of magnetic induction intensity. Finally, the inductance is flux divided by total current. In a reverse way, however, we can regard the L_i (inductance of i^{th} sub-port) as the magnetic flux and regard magnetic flux as a vector which has a direction perpendicular to equivalent current reference direction shown in Fig. 4(b). Then the process of calculation of total magnetic induction intensity by vector summation of respective magnetic induction intensity generated by sub-port current and integration of total magnetic induction intensity to obtain total flux is replaced by vector summation of respective sub-inductances. The equivalent one port network is shown in Fig. 4(c). This is the only conceptual definition of total inductance. From the simulation point of view, because excited current can be applied simultaneously at individual ports, total inductance can be easily simulated using circuit inductance definition. But using this circuit conception to experiment is not an easy thing. Even it can't be implemented. Therefore, there has no measurement method to obtain a total inductance of low laminated busbar up to now.

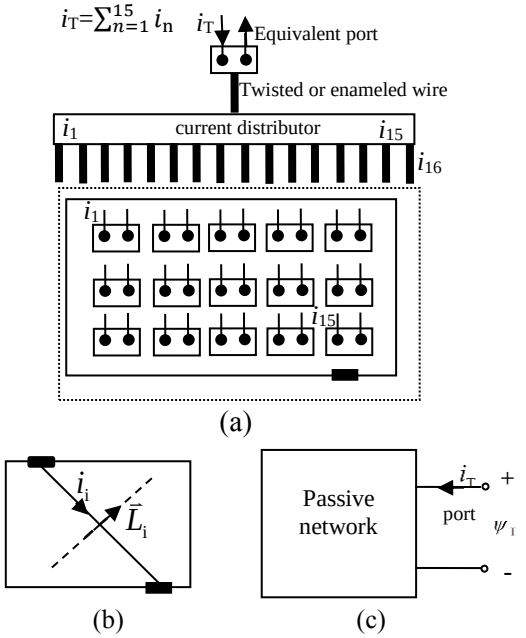

Fig. 4 (a) Definition of total inductance for a multi-port system. (b) Illustration of equivalent current direction and equivalent inductance direction of a vector synthesis method for an individual port. (c) Equivalent one port network of the multi-port system.

The orientation of the master reference frame can be chosen arbitrarily meaning y_0 must not point towards Port 19. This is because the function of the master reference frame is to provide a trigonometric relationship between all of the 15 individual reference frames and does not represent an alignment to Port 19.

In order to map a scalar product such as the inductor value L in a reference frame, the scalar product must be given a direction. Unit vectors $\vec{\imath}, \vec{\jmath}, \vec{k}$, commonly provide directions to scalar products in a three-dimensional space. Subsequently, each frame has its own unit vectors:

$$\vec{\imath}_k = \begin{pmatrix} 1 \\ 0 \\ 0 \end{pmatrix} \tag{7}$$

$$\vec{\jmath}_k = \begin{pmatrix} 0 \\ 1 \\ 0 \end{pmatrix} \tag{8}$$

$$\vec{k}_k = \begin{pmatrix} 0 \\ 0 \\ 1 \end{pmatrix} \tag{9}$$

Where $\vec{\imath}_k, \vec{\jmath}_k, \vec{k}_k$ are the unit vectors for each reference frame k (k=1 to 15) representing the positive direction x, y, and z respectively. A vector in each frame can be generally described as:

$$\vec{V}_k = a_k\vec{\imath}_k + b_k\vec{\jmath}_k + c_k\vec{k}_k \tag{10}$$

Where a_k, b_k and c_k are scalar products with respect to the unit vectors. In (1) it is shown that the magnetic field has only a y – orientation, therefore the scalar products a_k and c_k are zero. As the stray inductance described in (3) is the result of the magnetic field b_k becomes L_k and the vector can be written as,

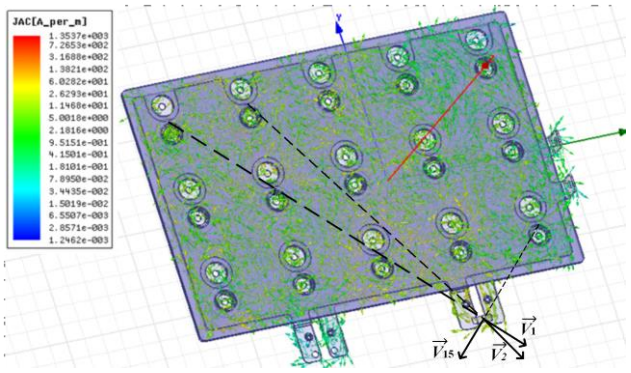

Fig. 5 Illustration of the direction of the unit vectors for $\vec{V}_1$, $\vec{V}_2$ and $\vec{V}_{15}$.

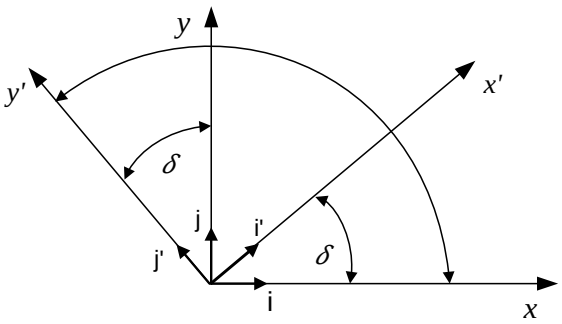

Fig. 6: Two-dimensional reference frame transformation

$$\vec{V}_k = 0\vec{\imath}_k + L_k\vec{\jmath}_k + 0\vec{K}_k = L_k\vec{\jmath}_k \tag{11}$$

Equation (11) describes the mapping of the stray inductance L_k into the frame k. L_k remains a scalar and the value is calculated from (3).

An illustration of the above is shown in Fig. 5 as an example. The three connections Port 1-Port 19, Port 2-Port 19 and Port 15-Port 19 are assumed as parallel flat inductors

resulting in the three vectors $\vec{V}_1$, $\vec{V}_2$ and $\vec{V}_{15}$.

Due to the flat structure w, $l_b >> p$ all the 15 reference frames (x_k-y_k-z_k) reduce from 3D to 2D. With z_k=0, the reference frames become (x_k-y_k). As mentioned earlier, to calculate the total stray inductance all the reference frames (x_k-y_k) must be aligned with one master reference frame (x_0-y_0) and Fig. 6 shows graphically a two-dimensional reference frame transformation.

The relationship between the two frames is described using the transformation matrix T which can be expressed as [25],

$$T = \begin{pmatrix} cos\delta & sin\delta \\ -sin\delta & cos\delta \end{pmatrix} \quad (12)$$

Each reference frame k has its own transformation matrix T_k:

$$\begin{pmatrix} x_0 \\ y_0 \end{pmatrix} = T_k \begin{pmatrix} x_k \\ y_k \end{pmatrix} \quad (13)$$

Due to the transformation the stray inductance L_k which is a single scalar component in reference frame k becomes a two scalar components L_{xk0} and L_{yk0} in the master reference frame:

$$\begin{pmatrix} L_{xk0} \\ L_{yk0} \end{pmatrix} = T_k \vec{V}_k = T_k L_k \begin{pmatrix} 0 \\ 1 \end{pmatrix} = \begin{pmatrix} cos\delta_k & sin\delta_k \\ -sin\delta_k & cos\delta_k \end{pmatrix} L_k \begin{pmatrix} 0 \\ 1 \end{pmatrix} \quad (14)$$

Leading to:

$$L_{xk0} = L_k sin\delta_k \quad (15)$$

$$L_{yk0} = L_k cos\delta_k \quad (16)$$

The total stray inductance can now be obtained by adding each component along the x_0 axis with each component along the y_0 axis divided by the total number of reference frames k. Thus, the total stray inductance in x_0 axis L_{xo} is,

$$L_{x0} = \sum_{k=1}^{15} L_k sin\delta_k \quad (17)$$

and the total stray inductance in y_0 axis L_{yo} is given as,

$$L_{y0} = \sum_{k=1}^{15} L_k cos\delta_k \quad (18)$$

By measuring the angles using the geometry of the position of the port with respect to the position of the master reference frame the total stray inductances can be calculated to

$$L_0 = \frac{\sqrt{L_{x0}^2 + L_{y0}^2}}{15} \quad (19)$$

Utilizing the stray inductances from Fig.2 the total stray inductances in x_0 and y_0 directions are calculated as $L_{x0} = 180.71\text{nH}$ and $L_{y0} = 482.57\text{nH}$ and the total stray inductance is obtained as,

$$L_0 = \frac{\sqrt{L_{x0}^2 + L_{y0}^2}}{15} = \frac{\sqrt{(180.71nH)^2 + (482.57nH)^2}}{15} = 34.353\text{nH} \quad (20)$$

Comparing the total stray inductance shown in (20) with the total stray inductance shown in Fig.2 there is only a marginal difference of 0.346 nH which is a clear indicator that our proposed method almost correctly calculates the total stray inductance by measuring the individual stray inductances.

Similarly, the total stray inductance of the busbar B is calculated as 40.856nH by using the method proposed above. Compared with the total stray inductance from the simulated result of 39.957 nH in Fig.2 for busbar B, the synthesized value of inductance is less than the simulated result with only a difference of 0.899nH, which successfully validate the effectiveness of the proposed method.

B. Analytical calculation of the contribution

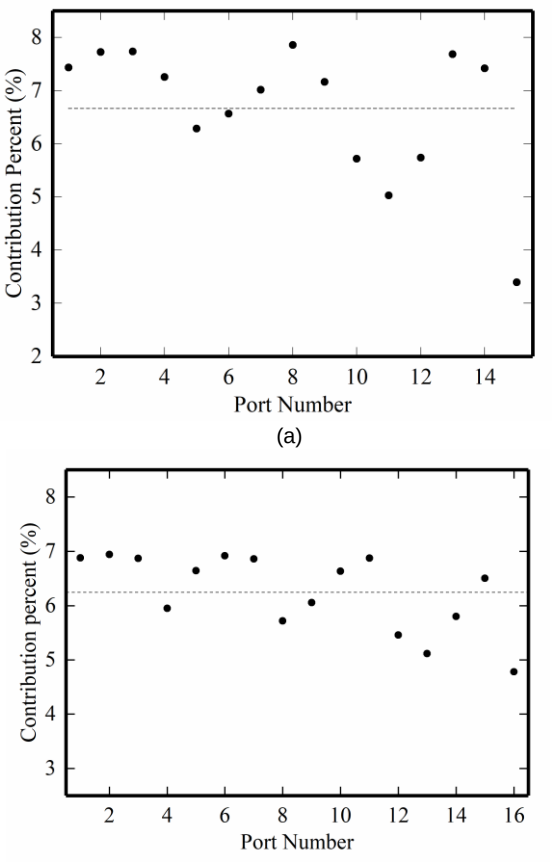

Fig. 7. Inductance contribution percentages of ports (a) busbar A (b) busbar B

The contribution percentages of different ports for busbar A can be analyzed according to the equation shown below,

$$\varepsilon = \frac{L_{kp}}{15L_0} \times 100\% \quad (21)$$

Where L_{kp} is a projection of kth inductance at the kth port on the direction of total inductance. The subscript of p denotes meaning of projection. On the low inductance busbar A, every row has five ports. According to (21), inductance contributions at different ports to the total stray inductance of busbar A and busbar B can be analyzed and the results are presented in the form of dispersed points as shown in Fig. 7. It can be seen that the ports located near borders contribute less inductance than those near center.

IV. MEASUREMENT OF INDUCTANCES

A. Connection Leads

Due to the low value of stray inductance of laminated planar busbars, the connection lead between the impedance analyzer and the ports plays an important role. On the one hand the inductance of the lead must be as small as possible, but on the other hand, the lead must be long enough to physically connect the equipment with the busbar. In order to understand the cause of the measurement error, four kinds of connecting leads are designed to connect to the impedance analyzer. The first lead is a twisted insulated lead with alligator terminals with a length of 230 mm as shown in the most left of Fig.8 (a). The second lead is a twisted insulated lead with copper cylinder terminals as shown in the second from left of Fig.8 (a), and it has the same length of 230 mm. The third lead is a closely parallel enamel lead and the fourth lead is a twisted enamel lead as shown in Fig.8 (a). Both of the lengths of lead No.3 and No.4 is 200 mm. These two leads are all with copper cylinder plates. Clips at the terminal of leads are used to connect to the port of the busbar whereas copper cylinder each at the terminal that can be physically inserted into the holes of the poles by imposing a light force on the cylinder contact. Two tests are conducted using the parallel enamel leads. In Test-A, as shown in Fig.8 (b), the terminals of the cylindrical contacts are put into the hole of the measuring port. In Test-B, as shown in Fig.8 (c), the terminals of the cylindrical contacts are put closely onto the poles of the measuring port.

(a)

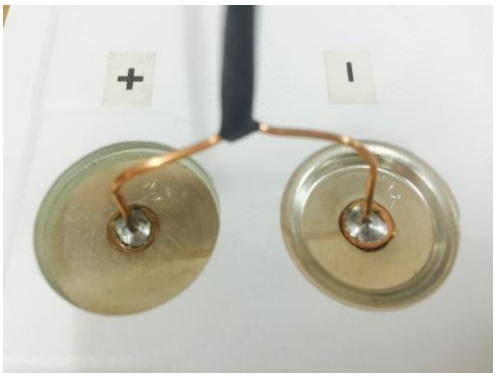

(b)

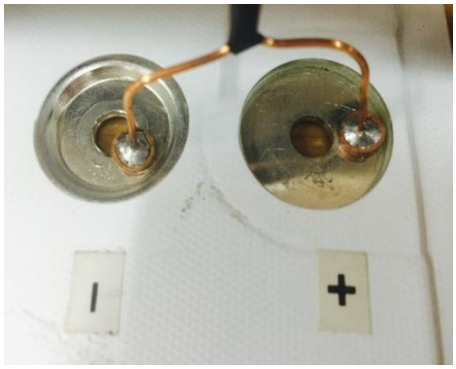

(c)

Fig. 8 (a) Twisted insulated leads with alligator clips, twisted insulated leads with a cylinder contacts, parallel enamel leads and twisted enamel leads, respectively, from left to right. (b) Test-A- measurement contacts are put into the poles of the measuring port. (c) Test-B- measurement contacts are put on the plane near the measured input port.

B. Compensation procedure

The impedance analyzer Agilent 4294A was used for this experiment. The 4294A covers a test-frequency range between 40 Hz to 110 MHz and can inject RMS voltages between 5mV and 1V. The impedance accuracy is stated as +/- 0.08% [26]. As with any impedance analyzer, the connection leads will impact on the measurement due to the lead residual impedance and stray admittance. In order to calculate these values, two tests must be conducted. The open circuit test provides the stray admittance value and the short circuit test provides the residual impedance value. The short link that has been used has a length of 39mm, a width of 7mm and thickness of 1mm. The inductance of this short link is subtracted automatically by the impedance analyzer during post-processing. Also, tests using twisted insulated leads were conducted. In addition to the automatic compensation by the impedance analyzer, measurement results can also be compensated manually. Some tests have been conducted to investigate the difference by using both compensation methods.

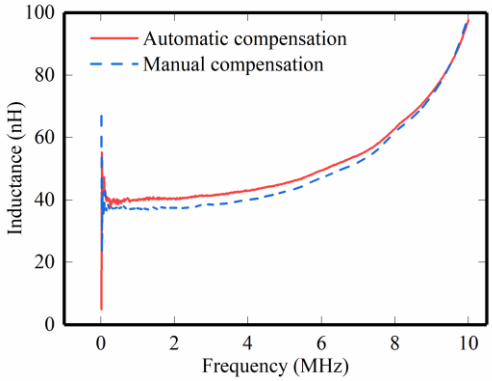

Fig. 9 The comparison of inductances using automatic and manual compensation for Port 1.

Fig. 9 illustrates a comparison of automatic and manual compensated measurement inductances for port 1, in which the manual measurement inductance is obtained by subtracting lead inductance from the total inductance. The twisted insulated lead is used as a connection in this study and

the results show that the inductance difference is stable with a small variation, about 2-3 nH at the frequency range of 40Hz-6MHz.

C. Experimental Results

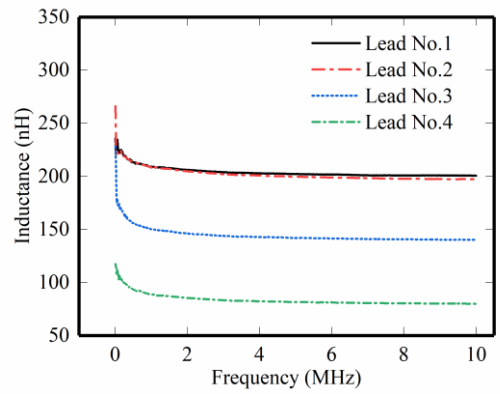

Fig. 10 The self-inductance of four kinds of leads

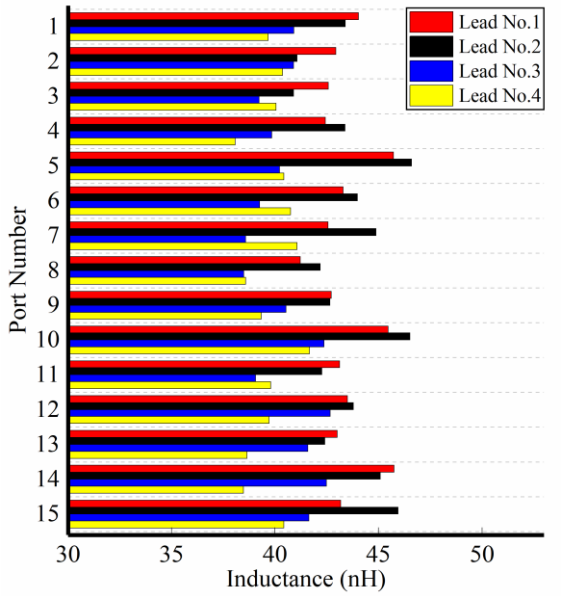

Fig.11 Measured stray inductances L1 to L15 using four kinds of lead （unit: nH）

The test results of self-inductance of four types of leads are shown in Fig. 10. It can be seen that the value of the twisted insulated lead with alligator clips is largest and it is basically the same as that of a twisted insulated lead with cylinder contacts. The self-inductance of parallel enamel lead indicates the smallest value and it is nearly one-third of the self-inductance of twisted insulated lead. The twisted insulated lead is widely used as a connection for electric measurement and its self-inductance is normally neglected in the measurement. However, this result shows that it cannot be the ideal connection lead for the low inductance measurement. Since the inductance to be measured is within a few dozen nano-Henry which is much smaller than the self-inductance. At low frequency stage internal self- inductance is proportional to reciprocal of square root of frequency. With the increase of frequency, due to skin effect penetration depth of electromagnetic field (EM) is obviously decreased. According to a depth of EM penetration of (22)

$$\delta=\sqrt{\frac{1}{2\pi f \mu\gamma}} \tag{22}$$

at a frequency of 841 kHz, depth of penetration of copper cylinder wire is 0.0508 mm, where the electrical conductivity γ is 5.8×10^7 S/m, the magnetic permeability of μ is $4\pi \times 10^{-7}$H/m, and frequency f is 841×10^3 Hz. With an increase in frequency, the depth of penetration is decreased and the internal self-inductance is reduced dramatically. At the frequency of 841 kHz, the internal self- inductance is very small which can be neglected and the self-inductance is only dominant by the external self-inductance. Therefore, at high frequency stage the self-inductances of four kinds of leads are basically constant. This can be verified by the results as shown in Fig. 10. In addition, because the thickness of insulation of the twisted insulated lead is much larger than the insulating coat of the enamel lead, the self-inductance of the twisted leads much large than that of the enamel lead.

The measured stray inductances for each port with different lead styles and connection points are summarized in Fig.11.

TABLE I
MEASURED STRAY INDUCTANCES L_1 TO L_{15} USING ENAMEL LEADS (TEST-A AND TEST-B) (UNIT: NH)

Port number	Test-A	Absolute error	Test-B	Absolute error
1	40.9066	-0.2884	43.3880	2.1930
2	40.8929	0.5759	42.7323	2.4153
3	39.2316	-0.3774	42.5484	2.9394
4	39.8389	0.1209	40.7275	1.0095
5	40.2130	-0.9160	40.9729	-0.1561
6	39.2578	-1.3452	41.0006	0.3976
7	38.5843	-0.3267	40.4940	1.5830
8	38.4930	-1.8090	41.3396	1.0376
9	40.5295	1.3195	40.7685	1.5585
10	40.3615	-2.1805	40.8374	-1.7046
11	37.0591	-3.0469	42.5085	2.4025
12	42.6704	3.2934	41.8359	2.4589
13	41.5910	-1.1500	40.4943	-2.2467
14	42.4809	1.8659	40.4613	-0.1537
15	41.6401	0.2761	41.4484	0.0844

The inductances measured by Test-A and Test-B and corresponding errors relative to simulated inductances at the respective port are given in Table I. It can be seen that from port number 1 to port number 11, the stray inductances measured using Test-A are always less compared to the stray inductance measured with Test-B with the biggest difference of 5.4494 nH at Port 11. And from port 12 to port 15 the stray inductances measured using Test-A are always larger compared to the stray inductance measured with Test-B with the biggest difference of 2.0196 nH at Port 14. These phenomena can be attributed to the variation of parameters of equivalent length of current and equivalent current width from (3). However, from the electromagnetic point of view, it is due to end effect and fringing effect. Since more input end effect is introduced in Test-B than Test-A, the inductances measured by Test-B are larger than that by Test-A from port 1 to port 11. The results also mean that the connection method to the busbar has much effect on the measurement of the stray inductances. This observation was already established through

simulation (Section II.B). The absolute errors, with respect to results by FEM analysis, are also given in Table. I. It is evident that the measured inductances by Test-A and Test-B are varied which relates to a specific position of each port. In reality, the capacitors are connected through the hole of the connection ports. Hence, Test-A is considered as the optimum connection since it is mimicking the real environment when it comes to excitation.

Fig. 12(a) presents the comparison of the measured inductances using both schemes of Test-A and Test-B at different frequencies for Port 1. The frequency range is from 40 Hz to 10 MHz in Fig. 12(a). From this figure, it can be observed that the stray inductances measured with Test-B are higher compared to Test-A. When the frequencies are above 1 MHz, the differences between them become nearly constant. Fig. 12(b) shows the inductances obtained by FEM simulation using both schemes of Test-A and Test-B at different frequencies at Port 1, where the inductances computed by scanned mode and by single frequency point are compared. It can be seen that the simulated inductances obtained by frequency scanning are larger than that by a single frequency method in both Test-A and Test-B.

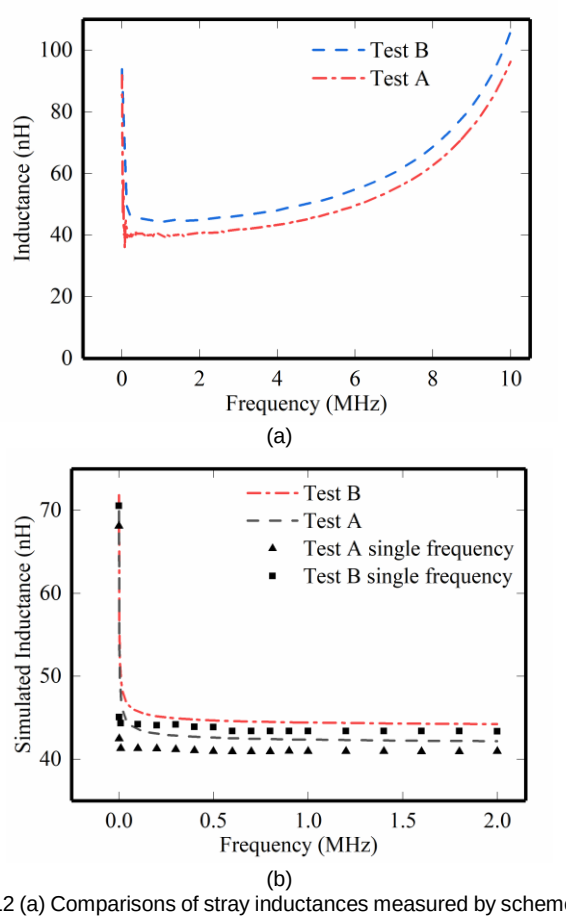

Fig. 12 (a) Comparisons of stray inductances measured by schemes of Test-A and Test-B using frequency scanning. (b) Comparisons of stray inductances simulated by FEM for schemes of Test-A and Test-B at different excitation frequencies.

V. Comparison between analytical work, FEM simulation and experimental results

By applying the proposed vector synthesis method, the synthesized stray inductances can be calculated using five schemes of measurement as listed in the second column of Table II. Compared with the simulated total inductances of 34.699nH in Fig.2, the absolute errors and relative errors are calculated and listed in third and fourth columns of Table II. These results show that the relative errors of synthesized inductances using parallel enamel leads are better than that using the other three leads.

Using (19) the total stray inductance is calculated as 34.0721 nH for Test-A and 35.1790nH for Test-B. The FEM simulation provides a total stray inductance of 34.699nH based on open holes in the ports that connect with the capacitors. Thus, the simulation results can be compared with Test-B results and the difference between them is just 0.48nH. This difference in Test-A is -0.6269 nH. Thus, the difference from Test-B is slightly smaller than that from Test-A. These results show that the proposed method can be successfully applied to determine the stray inductance almost accurately.

TABLE II
COMPARISON OF SYNTHESIZED STRAY INDUCTANCES FOR FIVE SCHEMES OF MEASUREMENT RELATIVE TO FEM SIMULATION (UNIT: nH)

	synthesized inductance	Absolute error	Relative error
Twisted lead	36.1581	1.4591	4.205%
Twisted lead with copper cylinder	36.6421	1.9431	5.601%
Parallel enamel lead (Test-A)	34.0721	-0.6269	-1.807%
Parallel enamel lead (Test-B)	35.1790	0.48	1.383%
Twisted enamel lead	33.472	-1.227	-3.536%

Placing the contacts ends of the enamel leads in the hole of the contact ports provides a more realistic environment (Test-A). Due to different injection of exciting currents of both schemes of Test-A and Test-B being different, their end effects on inductances are different. The stray inductance determined by Test-A is reduced by 1.1069 nH compared to when the contacts ends are placed beside the whole (Test-B). Results from the proposed method using Test-A and Test-B can also be compared with the classical measurement procedure which measures the stray inductance from the center of the busbar. Port 8 is the center of the busbar which reports values of 38.4930 nH for Test-A and 41.3396nH for Test-B. Comparing these values with the results obtained using the proposed method, i.e. 34.0721nH (Test-A) and 35.1790nH (Test-B) concludes that the proposed method increases the measurement accuracy by 11.5% when using Test-A and by 14.9% when using Test-B.

VI. Conclusions

A vector synthesis method to determine the stray inductance of low inductive laminated planar busbars by using

an impedance analyzer was proposed. The stray inductance from each capacitor port is measured and the value is mapped onto a *x-y-z* reference frame for each port. This mapping allows that each measurement can be vectored. Using the reference frame transformation theory, all the reference frames are aligned with one master reference frame. Subsequently, all the vectors undergo a transformation resulting in the calculation of the total stray inductance. The method was applied for two H-bridge low inductive laminated planar busbars that connect to 15 and 16 capacitors, respectively. FEM simulation shows that the busbars have stray inductances of 34.699nH and 39.957nH, respectively. The paper compares four different measurement methods to validate the proposed method based on busbar A with 15 input ports. The use of twisted insulated leads produced unsatisfactory results, and the enamel leads form the better option. Placing the contact ends of the enamel leads in the hole of the contact ports provides a more realistic environment (Test-A). The stray inductance for Test-A using the proposed method has a difference of 1.1069nH compared to when the contact ends are placed beside the hole (Test-B). Through comparison of self-inductance of the twisted insulated leads with that of the enamel leads, it can be proven that the enamel lead is more suitable for low inductance measurement due to its low value and increased measurement accuracy. When comparing the proposed method with the classical stray inductance measurement method (i.e. center-based measurement) the accuracy of the proposed method improves by 11.5% for Test-A and 14.9% for Test-B. The proposed method has so far been applied to planar structures. More research is required to investigate the accuracy of the method when applied to more complex bus bar structures.

REFERENCES

[1] [1] R. Shi, S. Semsar, and P. W. Lehn, "Constant Current Fast Charging of Electric Vehicles via a DC Grid Using a Dual-Inverter Drive," *IEEE Transactions on Industrial Electronics*, vol. 64, pp. 6940-6949, 2017.

[2] A. Kolli, O. Béthoux, A. De Bernardinis, E. Labouré, and G. Coquery, "Space-vector PWM control synthesis for an H-bridge drive in electric vehicles," *IEEE Transactions on Vehicular Technology*, vol. 62, pp. 2441-2452, 2013.

[3] F. Khoucha, S. M. Lagoun, K. Marouani, A. Kheloui, and M. E. H. Benbouzid, "Hybrid cascaded H-bridge multilevel-inverter induction-motor-drive direct torque control for automotive applications," *IEEE Transactions on Industrial Electronics*, vol. 57, pp. 892-899, 2010.

[4] M. N. Anwar and M. Teimor, "An analytical method for selecting DC-link-capacitor of a voltage stiff inverter," in *Industry Applications Conference, 2002. 37th IAS Annual Meeting. Conference Record of the*, 2002, pp. 803-810.

[5] ROLINX. (2015). *Laminated Busbar*. Available: https://www.rogerscorp.com/documents/4384/pes/rolinx/ROLINX-Laminated-Busbar-Design-Rules.PDF

[6] A. D. Callegaro, J. Guo, M. Eull, B. Danen, J. Gibson, M. Preindl, *et al.*, "Busbar Design for High-Power Inverters," *IEEE Transactions on Power Electronics*, vol. 33, pp. 2354-2367, 2018.

[7] M. C. Caponet, F. Profumo, R. W. De Doncker, and A. Tenconi, "Low stray inductance busbar design and construction for good EMC performance in power electronic circuits," *IEEE Transactions on Power Electronics*, vol. 17, pp. 225-231, 2002.

[8] Q. Liu, S. Wang, A. C. Baisden, F. Wang, and D. Boroyevich, "EMI suppression in voltage source converters by utilizing dc-link decoupling capacitors," *IEEE Transactions on Power Electronics*, vol. 22, pp. 1417-1428, 2007.

[9] K. Fink and S. Bernet, "Advanced Gate Drive Unit With Closed-Loop diC/dt Control," *IEEE Transactions on Power Electronics*, vol. 28, pp. 2587-2595, 2013.

[10] F. Zare and G. F. Ledwich, "Reduced layer planar busbar for voltage source inverters," *IEEE Transactions on Power Electronics*, vol. 17, pp. 508-516, 2002.

[11] Z. Lounis, I. Rasoanarivo, and B. Davat, "Minimization of wiring inductance in high power IGBT inverter," *IEEE Transactions on Power Delivery*, vol. 15, pp. 551-555, 2000.

[12] S. Jahdi, O. Alatise, L. Ran, and P. Mawby, "Accurate analytical modeling for switching energy of PiN diodes reverse recovery," *IEEE Transactions on Industrial Electronics*, vol. 62, pp. 1461-1470, 2015.

[13] L. Popova, T. Musikka, R. Juntunen, M. Lohtander, P. Silventoinen, O. Pyrhönen, *et al.*, "Modelling of low inductive busbars for medium voltage three-level NPC inverter," in *Power Electronics and Machines in Wind Applications (PEMWA), 2012 IEEE*, 2012, pp. 1-7.

[14] S. Li, L. M. Tolbert, F. Wang, and F. Z. Peng, "Stray inductance reduction of commutation loop in the P-cell and N-cell-based IGBT phase leg module," *IEEE Transactions on Power Eectronics*, vol. 29, pp. 3616-3624, 2014.

[15] A. Datta and G. Narayanan, "Measurement of Parasitic Inductances in the Bus-Bar Assembly of a High Power Voltage Source Converter," *Journal of The Institution of Engineers (India): Series B*, vol. 97, pp. 537-547, 2016.

[16] C. Chen, X. Pei, Y. Chen, and Y. Kang, "Investigation, evaluation, and optimization of stray inductance in laminated busbar," *IEEE Transactions on Power Electronics*, vol. 29, pp. 3679-3693, 2014.

[17] B. Waltrip and F. Seifert, "A programmable capacitor for inductance measurements," *IEEE Transactions on Instrumentation and Measurement*, vol. 66, pp. 1572-1578, 2017.

[18] R. M. G. Salvador, J. A. G. Parra, and N. N. Castellano, "Characterization and modeling of high-value inductors in ELF band using a vector network analyzer," *IEEE Transactions on Instrumentation and Measurement*, vol. 62, pp. 415-423, 2013.

[19] K. Technologies. (2016). *Impedance Measurement Handbook - A guide to measurement technology and techniques 6th Edition*. Available: http://literature.cdn.keysight.com/litweb/pdf/5950-3000.pdf

[20] C. Geng, F. He, J. Zhang, and H. Hu, "Partial Stray Inductance Modeling and Measuring of Asymmetrical Parallel Branches on the Bus-Bar of Electric Vehicles," *Energies*, vol. 10, p. 1519, 2017.

[21] Z. Wang and G. Chen, "Study on planar busbar regarding stray inductance minimization and oscillation suppression for high power converter," in *Sustainable Power Generation and Supply, 2009. SUPERGEN'09. International Conference on*, 2009, pp. 1-7.

[22] K. Technologies. (2017). *LCR Meters, Impedance Analyzers and Test Fixtures*.Available: http://literature.cdn.keysight.com/litweb/pdf/5952-1430E.pdf

[23] P. A. Vasilevskii, L. M. Zheleznyak, M. Y. Borodin, and K. Y. Mal'tseva, "Preparation of Copper Electrical Engineering Alloy Strip with High Service Properties," *Metallurgist*, vol. 57, pp. 352-358, 2013.

[24] L. Lombardi, D. Romano, and G. Antonini, "Accurate and efficient low-frequency solution of partial element equivalent circuit models," *IEEE Transactions on Electromagnetic Compatibility*, vol. 59, pp. 1514-1522, 2017.

[25] S. Widnall. (2009). *Vectors, Matrices and Coordinate Transformations*.Available: https://ocw.mit.edu/courses/aeronautics-and-astronautics/16-07-dynamics-fall-2009/lecture-notes/MIT16_07F09_Lec03.pdf

[26] K. Technologies. *Agilent 4294A Precision Impedance Analyzer Data Sheet*.Available: https://literature.cdn.keysight.com/litweb/pdf/5968-3809E.pdf?id=1000072161:epsg:dow

Binxian Lu was born in Jiamusi, Heilongjiang, in 1969. He received Ph.D. degree in electrical power engineering from North China Electric Power University, Beijing, China, in 2007 and the M.S. degree in electrical power engineering from Harbin Institute of Technology, Harbin, China, in 1996.

He is currently a professor with North China Electric Power University. He is a Member of Beijing Key Laboratory of High Voltage and EMC, North China Electric Power University and a guest professor of the State Key Laboratory of Advanced Power Transmission Technology (Global Energy Interconnection Research Institute). From 2009 to 2010, he was a visiting scientist with University of Illinois, Urbana, USA. He is the author of 100 peer reviewed papers. His research interests include corona discharge, multi-physics field analysis in electric machine, electro-chemistry corrosion and deposition in HVDC, VFTO analysis in GIS, electromagnetic compatibility in power system, electromagnetic measurement, and electromagnetic numerical computation.

Volker Pickert (M'04) studied Electrical and Electronic Engineering at the Rheinisch-Westfaelische Technische Hochschule (RWTH), Aachen, Germany and Cambridge University, UK. He received his Dipl.-Ing. degree In electrical and electronic engineering from RWTH in 1994 and the Ph.D. degree in power electronics from Newcastle University, Newcastle upon Tyne, U.K. in 1997.

From 1998 to 1999, he was Application Engineer with Semikron GmbH, Nuremberg, Germany and from 1999 to 2003 he was Group Leader at Volkswagen AG, Wolfsburg, Germany, responsible for the development of electric drives for electric vehicles. In 2003 he was appointed as a Senior Lecturer in the Electrical Power Research Group at Newcastle University and in 2011 he became Full Professor of Power Electronics. In 2012 he has become the Head of the Electrical Power Research Group. He has published more than 120 book chapters, journal and conference papers in the area of power electronics and electric drives. His current research interests includes power electronics for automotive applications, thermal management, health monitoring techniques and advanced nonlinear control.

Prof. Pickert is the recipient of the IMarEST Denny Medal for the best article in the Journal of Marine Engineering in 2011. He was chairman of the biannual international IET conference on Power Electronics, Machines and Drives in 2010 in Brighton and he is the active Editor-in-Chief of the IET Power Electronics journal.

Junzhu Hu was born in Luoyang, Henan, in 1991. She received M.S. degree in electrical power engineering from North China Electric Power University, Beijing, China, in 2016.At present, she is working as an assistant engineer for State Grid Beijing Electric Power Company.

Her research interest mainly focuses on electromagnetic compatibility in power system, electromagnetic measurement and electromagnetic numerical computation.

Haimeng Wu (M'10) was born in Zhejiang, China, in 1986. He received the B.Sc. degree in electrical engineering from Chongqing University, Chongqing, China, in 2008. He obtained postgraduate recommendation with 1st class scholarship to Zhejiang University and then he received the M.Sc. degree in power electronics from College of Electrical Engineering, Zhejiang University, Hangzhou, China, in 2011. Then he received the grants from Engineering and Physical Science Council (EPSRC) for his further education in UK. In 2016, he received his Ph.D. degree in power electronics at the School of Engineering, Newcastle University, United Kingdom.

Dr. Wu joined in Electrical Power Research Group at Newcastle University as a Postdoctoral Researcher since 2015. He is the winner of Siemens European TAPAS Community Challenge Competition 2018. His current research interests include power electronics for electric vehicles, health management of wide band gap (WBG) device and wireless power transfer.

R. T. Naayagi (M'12–SM'15) is currently an Associate Professor in Electrical Power Engineering at Newcastle University in Singapore (NUiS). Her research interests include power electronic solutions for renewable energy integration, electric vehicle and aerospace applications.

Dr Naayagi has received several merit certificates and awards for her academic proficiency. She received the IET Woman Engineer Award and the Newcastle University Teaching Award. She is a Senior Member of the IEEE and a Fellow of the Higher Education Academy, UK. She an Equality & Diversity Champion for NUiS and Academic Lead for Athena SWAN Initiative. She is the Chair of NUiS WISE network and has been organizing many events to promote young women in engineering. She is the Chairman of the IEEE Power and Energy Society, Singapore Chapter. She is an Associate Editor for IET Power Electronics journal and serves as a Reviewer for the IEEE/IET/many other international journals and conferences.

Wei Kang was born Beijing, China, in 1983. He received the M.Eng. degree in electrical power engineering from North China Electric Power University, Beijing, China, in 2015.

His research interest mainly focuses on the structure of electrical equipment.

Sizhuo Liao was born in Jingmen, Hubei, China, in 1995. She received the B.Eng. degree in communication engineering from the School of Electrical and Electronic Engineering, North China Electrical Power University, Beijing, China, in 2016, where she is currently working toward the M.Eng. degree in electrical engineering.

Her research interest mainly focuses on the electromagnetic numerical computation and electromagnetic measurement.